

Desalination of seawater by spray freezing in a natural draft tower

Liu, Y., Ming, T., Wu, Y., Richter, R., Fang, Y. & Zhou, N.

Author post-print (accepted) deposited by Coventry University's Repository

Original citation & hyperlink:

Liu, Y, Ming, T, Wu, Y, Richter, R, Fang, Y & Zhou, N 2020, 'Desalination of seawater by spray freezing in a natural draft tower', *Desalination*, vol. 496, no. 1, 114700.

<https://dx.doi.org/10.1016/j.desal.2020.114700>

DOI 10.1016/j.desal.2020.114700

ISSN 0011-9164

Publisher: Elsevier

NOTICE: this is the author's version of a work that was accepted for publication in *Desalination*. Changes resulting from the publishing process, such as peer review, editing, corrections, structural formatting, and other quality control mechanisms may not be reflected in this document. Changes may have been made to this work since it was submitted for publication. A definitive version was subsequently published in *Desalination*, 496:1 (2020) DOI: 10.1016/j.desal.2020.114700

© 2020, Elsevier. Licensed under the Creative Commons Attribution-NonCommercial-NoDerivatives 4.0 International

<http://creativecommons.org/licenses/by-nc-nd/4.0/>

Copyright © and Moral Rights are retained by the author(s) and/ or other copyright owners. A copy can be downloaded for personal non-commercial research or study, without prior permission or charge. This item cannot be reproduced or quoted extensively from without first obtaining permission in writing from the copyright holder(s). The content must not be changed in any way or sold commercially in any format or medium without the formal permission of the copyright holders.

This document is the author's post-print version, incorporating any revisions agreed during the peer-review process. Some differences between the published version and this version may remain and you are advised to consult the published version if you wish to cite from it.

1

2 Desalination of seawater by spray freezing in a natural draft tower

3 Yang Liu^{1,2}, Tingzhen Ming^{1,3}, Yongjia Wu¹, Renaud de Richter⁴, Yueping Fang⁵, Nan Zhou³4 1. School of Civil Engineering and Architecture, Wuhan University of Technology, Wuhan 430070,
5 China.

6 2. Department of Mechatronic Engineering, Wuhan Business University, Wuhan, China.

7 3. China Energy Group, Environmental Energy Technologies Division, Lawrence Berkeley

8 National Laboratory, 1 Cyclotron Road, Berkeley, CA 94720 USA.

9 4. Tour-Solaire.Fr, 8 Impasse des Papillons, F34090 Montpellier, France.

10 5. Centre for Research in the Built and Natural Environment, School of Energy, Construction and
11 Environment, Coventry University, Priory Street, CV1 5FB Coventry, UK.

12

13 Corresponding Author :

14 Tingzhen Ming : School of Civil Engineering and Architecture, Wuhan University of Technology,
15 Wuhan 430070, China. Email : tzming@whut.edu.cn

16

17 **Abstract**

18 The freeze-melting process can be a viable method for the purposes of desalination
19 because of its low energy consumption, ignorable corrosion issues, and without huge
20 pressure or membrane replacement work. Large contact area for heat and mass transfer
21 per unit mass of water between the water and air and low heat resistance results in
22 higher energy efficiency during spray freezing desalination process compared to other
23 freezing desalination methods. A 200m high desalination tower was proposed in this
24 paper that could generate 27.7 kg/s fresh water in the form of water droplets with
25 2mm diameter at an atmospheric temperature of -26°C . This research has founded that
26 the natural convective airflow induced by the heat released by the warm water in the
27 freezing process could generate through the wind turbine mounted in this system
28 approximately one-third of the energy consumed by the water pump of the system. This
29 free energy has never been studied in previous research. The power consumption
30 required to produce 1 m^3 fresh water in this system is approximately 1.07 kWh .
31 Compared to traditional desalination methods, the power consumption of our new spray
32 freezing desalination system is much lower than previous systems with the same mass
33 flow rate of fresh water. Only 375.4 kJ cold energy to produce one-kilogram fresh
34 water. Thus, this spray freezing desalination system could be employed in desalination
35 industry if free cold energy (e.g. from the cold atmosphere or the regasification process
36 of LNG) and seawater resources are available.

37

38 **Keywords:**39 Compressible airflow; Natural draft tower; Seawater desalination; Spray freezing;
40 Water droplet

Nomenclature	
A	Heat (mass) transfer area per tower unit volume (m^2/m^3)
A_d	Surface area of a water droplet (m^2)
Bi	Biot number
C_d	Drag coefficient
$C_{p,B}$	Specific heat capacity of dry air ($\text{J}/\text{kg}\cdot\text{K}$)
$C_{p,w}^g$	Specific heat capacity of water vapor ($\text{J}/\text{kg}\cdot\text{K}$)
$C_{p,w}^L$	Specific heat capacity of liquid water ($\text{J}/\text{kg}\cdot\text{K}$)
d	Diameter of a water droplet (m)
D	Diameter of the tower (m)
$D_{w,a}$	Diffusivity of water vapor in air (m^2/s)
fr_{ice}	Ice mass fraction
F	Force (N)
F_r	Froude number
g	Gravitational acceleration, 9.81 (m/s^2)
G_B	Mass flow rate of dry air per unit cross-section area ($\text{kg}/\text{m}^2\cdot\text{s}$)
h	Tower height (m)
h_{conv}	Convective heat transfer coefficient ($\text{W}/\text{m}^2\cdot\text{K}$)
h_{mass}	Mass transfer coefficient ($\text{kg}/\text{s}\cdot\text{m}^2\cdot(\text{kg}/\text{kg})^{-1}$)
H_d	Specific enthalpy of a droplet (J/kg)
H_G	Specific enthalpy of moist air per unit mass of dry air (J/kg)
ΔH_s	Specific latent heat of fusion (J/kg)
H_w	Specific enthalpy of the liquid phase (J/kg)
ΔH_v	Specific heat of vaporization of water (J/kg)
k	Thermal diffusivity ($\text{W}/\text{m}\cdot^\circ\text{C}$)
L	Mass flowrate of water per unit cross-section area ($\text{kg}/\text{m}^2\cdot\text{s}$)
M	Mach number
M_a	Molar mass of moist air (kg/kmol)
m_d	Mass of a water droplet (kg)
m_w	Mass flow rate of the feed water (kg/s)
N	Number of water drops falling through a unit volume per second
Nu	Nusselt number
P	Air static pressure (Pa)
P_r	Prandtl number
$P_{w,sat}$	Vapor pressure of the seawater (Pa)
q	Heat-transfer flux (w/m^2)
Q	Heat transferred per unit mass (w/kg)
R	Specific gas constant for air, 287 ($\text{J}/\text{kg}\cdot\text{K}$)
Re	Reynolds number
S_h	Sherwood number
t	Time (s)
T	Temperature (K)
v	Velocity (m/s)
Y_w	Humidity mass ratio of moist air (kg/kg)
$Y_{w,i}$	Humidity mass ratio at the gas-phase side of interface (kg/kg)
z	Height from the bottom of the tower (m)
Greek symbols	
α	Thermal diffusivity (m^2/s)
γ	Specific heat ratio of air
ε	Pressure loss coefficient
ζ	Turbine pressure drop factor
η	Mechanical efficiency of turbine generator
λ	Friction coefficient on the wall in the tower
ρ	Air density (kg/m^3)
μ	Dynamic viscosity ($\text{Pa}\cdot\text{s}$)
Δ	Difference
Subscripts	
a	air
b	buoyancy
br	internal bracing
d	droplet
da	dry air
f	freezing point
g	gravitational
in	inlet
ice	ice
k	kinetic energy
la	lapse rate
$loss$	loss
n	nucleation
out	outlet
pot	potential
tur	turbine
w	water
∞	atmosphere
0	sea level
Shorthand with no physical meaning	
MX	

S	Cross-section area of the tower (m ²)	EX
S_c	Schmidt number	EXw

42 **1. Introduction**

43 Water resources are unevenly distributed on the global. Shortage of affordable
44 clear water is one of the most severe problems in many parts of the world with high
45 population density or rapid industrialization. However, many of these areas located near
46 to the huge water resources - seawater, for instance, Singapore, Alaska, and North
47 China [1-3]. Low-cost and high-quality water can be exploited by desalination from the
48 seawater to meet the urgent demand of daily consumption of a huge population and for
49 future industrial development.

50 When seawater is freezing, ice tends to exclude the impurities during the
51 crystallization process. For instance, the natural-growth sea-ice has a much lower salt
52 content than the original seawater and is drinkable for human after it thaws. This
53 phenomenon was found by sailors and the inhabitants living in polar regions [4]. Freeze
54 desalination consumes less energy input by 6-7 times compared to the evaporative
55 crystallization process due to the larger latent heat of vaporization compared to that of
56 solidification [5]. Also, freeze desalination with no need for ancillary chemicals [4] is
57 more environmental-friendly compared to the evaporative crystallization process. In
58 addition, compared to the Reverse Osmosis method, the freezing melting process does
59 not need huge pressure or membrane replacement [4, 6]. Furthermore, the freeze
60 desalination is insensitive to corrosion problems because of its low operating
61 temperature [7]. Following the freeze desalination process, the treatments such as
62 gravity drainage, crushing, centrifugation, filtering, washing by fresh water or even
63 microwave treatment can further improve the quality of ice by breaking the “ice-salt
64 pocket” in the ice and releasing the concentrated brine out of the ice [8-10]. In addition
65 to the above advantages, the freeze-melting process will be more economic and
66 attractive for freezing seawater if waste or renewable energy is used to freeze the
67 seawater.

68 Cao, et al.[11] utilized the cold (waste) energy released from the regasification
69 process of the LNG (liquefied natural gas) by a flake ice maker to desalinate seawater,
70 which generated 2kg ice with 1kg LNG re-gasification. Chang, et al. [3] desalinated the
71 seawater using the cold energy of LNG by the freezing process in Singapore. The total
72 dissolved solids at around 300 ppm were achieved by washing in the final product,
73 which meets the salinity of 500 ppm of WHO potable water standard. Wang and Chung
74 [12] developed a hybrid desalination process comprising freeze desalination (cold
75 energy from LNG) and membrane distillation processes. High-quality drinkable water
76 with a low salinity of 0.104 g/L was obtained in the freeze desalination process alone.
77 Combined with freeze desalination, the membrane distillation process was employed
78 to treat the brine discharged from the freeze desalination unit. Drinkable clean water
79 was successfully produced by the hybrid process with a total water recovery of 71.5%.

80 John, et al. [13] even proposed to purify the urban wastewater by the natural freeze.
81 With this method, no cold energy input was needed and 95% purification efficiency
82 was achieved. Once free cold energy is available, there is potential to generate clear
83 water by the freeze desalination method.

84 Some devices were specially designed for crystallizing the salt solution to generate
85 ice and solid salt simultaneously. A novel 151 freezing disk column crystallizer has
86 been built to separate the frozen salt solution into ice and salt under the eutectic freezing
87 point [14]. With this device, as a case study, a 35 w% aqueous sodium nitrate and a 12
88 w% copper sulfate stream fed into the disk column crystallizer were cooled down to
89 the eutectic freezing point to separate water and salt. Compared to conventional multi-
90 step evaporation, the energy reductions by using freeze desalination are 30% of that of
91 sodium nitrate and 65% of that of copper sulfate [15].

92 Although it has been demonstrated that the freeze-melting process could be a
93 method for desalination, the block, layer, or falling film freeze processes are not energy-
94 efficient. Large thermal resistance exists due to the wall of the heat exchanger, the water,
95 or the ice itself, which results in a low rate of heat transfer and long crystallization time.
96 So, a direct freezing method - spray freezing with a large area of heat transfer with a
97 low thermal resistance is preferred in the freeze-melting process. During the spray
98 freezing process, the water droplets are sprayed directly into the cold air to be frozen.
99 The large surface area per unit volume of water drops makes the rates of both cooling
100 and ice formation much faster.

101 When the seawater is pumped and sprayed into the cold air, the surface
102 temperature of water droplets falls below ice nucleation temperature, they solidify from
103 the outside and push the impurities to the center of the drop by crystallization front,
104 resulting in a higher concentrated liquid and nearly pure ice [16]. The outer shell
105 fracture, when droplets fall and contact with the cold ground. The built-up pressure
106 inside the droplet caused by phase change expansion can also rupture the ice shell, and
107 release the liquid impurities out of the droplet [17]. The excess water drained out from
108 a spray ice deposit becomes runoff that is more concentrated than the original seawater.

109 The spray freezing process was proposed to produce drinkable water in Alaska in
110 the 1960s, which achieved salt concentration in the ice 0.007 times lower than the
111 source seawater [2]. The spray freezing was also used to treat pulp mill effluent and oil
112 sands tailings pond water by Gao, et al. [18]. In Gao's experiment, greater than 60%
113 impurity reduction in the spray ice was obtained when 30% of the total volume of the
114 sprayed water was released as runoff. Another field experiment was conducted to
115 evaluate the efficiency of spray freezing to remove dissolved chemicals from the lake
116 of tailing water at the Colomac Mine. The experimental analysis showed that after the
117 initial 39% of the spray ice column had been melted, the efficiency of dissolved
118 chemical removal in the ice core reached up to 87-99% [19]. Tatarniuk, et al. [20] used
119 spray freeze separation to concentrate salt in snowmelt water gathered from snow

120 runoff water on the roads into higher concentrated reusable brine to recover and recycle
121 salts, intending to drive down salt costs in the Canadian winter. The spray freezing
122 could concentrate the water 1.3~1.4 times higher than the source water, with much
123 purer ice mound left.

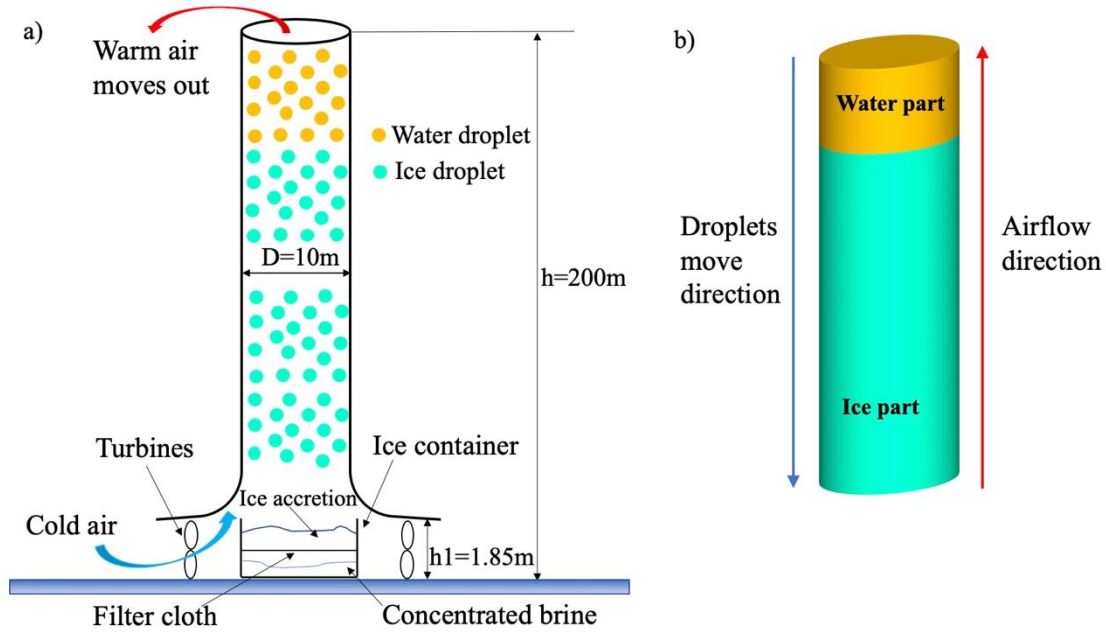
124 Although the spray freezing to purify water is proved to be feasible, a large-scale
125 continuously-running spray freezing system has not been proposed. The heat and mass
126 transfer mechanism during the spray freezing and the impact factors in this spray
127 freezing process have not been analyzed yet. Besides, in a large-scale continuously-
128 running spray freezing system, the heat energy released from the water droplets during
129 its freezing was never utilized in the previous research. Actually, this energy is a kind
130 of heat that could heat the cold air and form natural air current which can be utilized in
131 a spray freezing tower to propel the turbines mounted on the top of the tower to generate
132 electricity (see Fig. 1). So, the main objective of this paper is to desalinate seawater by
133 spray freezing utilizing the free cold energy from the atmosphere (or from LNG) and
134 generate green power simultaneously. An economic analysis of this method compared
135 with freezing by a heat-exchanger is also undertaken in this paper.

136

137 **2. Principle of the spray freezing desalination**

138 To freeze the sprayed seawater droplets and utilize the free heat energy released
139 by the water, a 200m high spraying tower with turbines mounted at the bottom is
140 introduced in this paper. The warm seawater droplets are sprayed from the top of the
141 tower, the freely-falling droplets would release heat into the air inside the tower. The
142 heated air in the tower would float upwards because of its lower density, which caused
143 a natural air draft. The updraft can be used to propel the turbines to generate electricity.

144 At the upper part of the tower, the droplets will be in the liquid state. When the
145 temperature of droplets reduces to the freezing temperature, they will be frozen and
146 become ice particles. If the droplets are partially frozen, the mixture of ice and
147 concentrated brine is collected by the ice container at the bottom and filtered. Pure ice
148 will be separated from brine and stored to produce fresh water. The concentrated brine
149 will drain off. This proposed spray freezing desalination is presented in Fig. 1. The
150 geometrical parameters of this system are derived from [21].



151

152

153

154

155

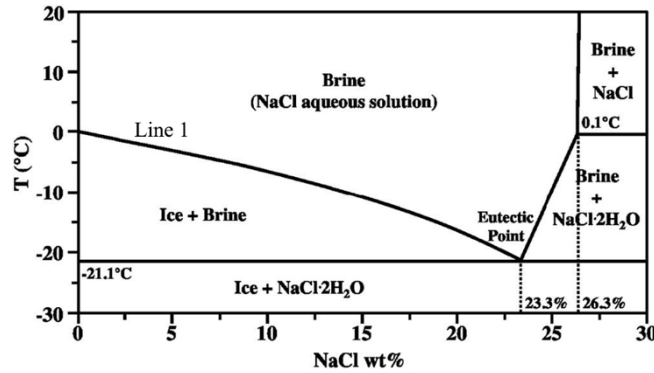
156

157

158

Fig. 1. (a) Schematic diagram of the spray freezing desalination system, (b) flow directions of seawater droplets and air.

The principle of desalination by freeze crystallization can be described by the typical phase diagram of binary solution which represents the equilibrium lines between solid and liquid states of materials. A schematic representation of the phase change diagram of saline water (NaCl-H₂O) is depicted in Fig 2. Line 1 defines the freezing point of water at different sodium chloride mass content.



159

160

161

162

163

164

165

166

167

168

169

Fig. 2. Phase diagram for the NaCl solution as a function of temperature and salt concentration [22].

The starting point is on the left side of the eutectic point when the mass fraction is lower than 23.3wt%. The unsaturated saline solution is cooled until reaching the equilibrium point on Line 1. Further cooling will take the solution along Line 1 with equilibrium temperature depressing and concentration in remain liquid increasing until the eutectic point is reached at -21.1°C for NaCl solution.

The freezing point depression, T_f , depends linearly on the concentration of the salt and can be calculated as [23]:

$$T_f = -54.1126 \left(\frac{S_w}{1 - S_w} \right), -7.7 \leq T_a \leq 0^{\circ}\text{C} \text{ and } 0 \leq S_w \leq 12.47\% \quad (1)$$

where S_w is the salinity of the seawater (0.035 for the initial salinity before

170 desalination).

171

172 3. A single water droplet freezes in the tower

173 3.1 A single water droplet velocity

174 As the heat and mass transfer rate between the water droplets and the surrounding
175 air is decided by the drops' velocity, the velocity of the drops must be analyzed first. In
176 this work, the water drops were assumed to be spherical [24] and fall vertically in the
177 one-dimensional model. The forces exerted on one droplet include gravity F_g , buoyancy
178 from the air F_b , air friction drag F_a . The force balance equation is:

$$179 \quad m_d \frac{dv_w}{dt} = F_g - F_b - F_a \quad (2)$$

180 Where v_w = velocity of a water droplet, t = time (s).

181 The mass of a water droplet m_d can be calculated by $m_d = \pi d^3 \rho_w / 6$, the
182 gravitational force of a droplet is $F_g = \pi d^3 g \rho_w / 6$ and the buoyancy is $F_b = \pi d^3 g \rho_a / 6$.
183 The drag force by air friction F_a is expressed as $F_a = \pi C_d \rho_a (v_a + v_w)^2 d^2 / 8$. The
184 ρ_w and ρ_a represent the density of water and air, respectively. Then the motion
185 equation of the water droplet can be written as [25]:

$$186 \quad \frac{dv_w}{dt} = g \left(1 - \frac{\rho_a}{\rho_w} \right) - \frac{3 C_d \rho_a}{4 d \rho_w} (v_a + v_w)^2 \quad (3)$$

187 For liquid droplets, the following drag coefficient correlations were adopted [26]:

$$188 \quad C_d = \begin{cases} \frac{24.0}{Re}, Re \leq 1 \\ \frac{24.0}{Re} (1 + 0.15 Re^{0.687}), 1 < Re \leq 1000 \\ 0.44, Re > 1000 \end{cases} \quad (4)$$

189 where Re is the Reynolds number, $Re = \rho_a (v_a + v_w) d / \mu_a$.

190 The thermophysical properties of seawater and air needed for the numerical
191 calculation are listed in Table 1.

Table 1

Parameter quantities and correlations used.

Parameter	Quantity/correlation	Units	References
S_w	35	g/kg	[27]
$T_f^{1,2}$	$-54.1126 \left(\frac{S_w}{1 - S_w} \right)$	$^{\circ}C$	[23]
ρ_w	$1000 + 0.8 S_w$	kg/m^3	[23]
$C_{p,w}^L$	$1.005 - 0.004136 S_w + 0.0001098 S_w^2 - 0.000001324 S_w^3$	$Cal/g \cdot ^{\circ}C$	[23]
ΔH_v^3	2498510 ($0^{\circ}C, salinity 3.5\%$)	J/kg	[27]
ΔH_s^3	329928 ($salinity 3.5\%$)	J/kg	[27]
$P_{w,sat}^3$	602.4 ($0^{\circ}C, salinity 3.5\%$)	Pa	[27]

ρ_a	$\frac{P \cdot M_a}{8.3145 \times 10^3 T_a}$	kg/m^3	[28, 29]
M_a	$(1 + Y_w) / \left(\frac{Y_w}{18.015} + \frac{1}{28.966} \right)$	$kg/kmol$	[28, 29]
$D_{w,a}$	$2.227 \times 10^{-5} \left(\frac{T_a + 273.15}{273.15} \right)^{1.81}$	m^2/s	[23, 29]
μ_a	$\mu_0 \left[\frac{416.16}{T_a + 393.15} \left(\frac{T_a + 273.15}{296.16} \right)^{1.5} \right]$	$Pa \cdot s$	[23]
	$\mu_0 = 1.8325 \times 10^{-5} Pa \cdot s$		
α_a	$\frac{1}{(57736 - 585.78T_a)}$	m^2/s	[23, 29]
κ_a	$0.024577 + 9.027 \times 10^{-5} T_a$	$W/m \cdot ^\circ C$	[23, 29]

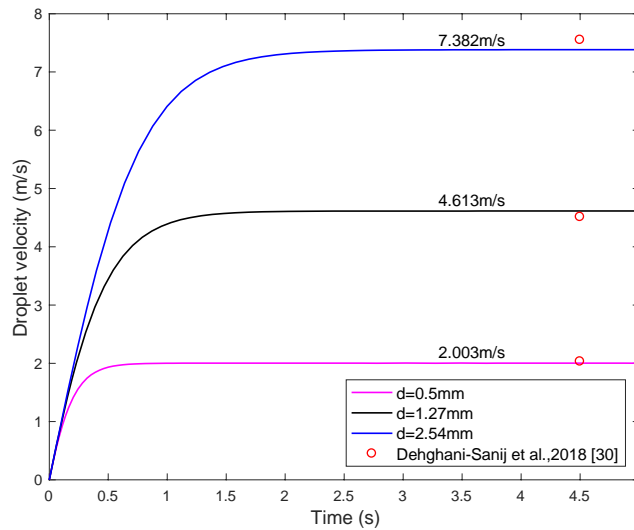
¹ The equation is valid in $-7.7 \leq T_a \leq 0^\circ C$ and $0 \leq S_w \leq 12.47\%$.

² The salinity, S_w , appears as a fraction in this formula (0.035 for Standard Ocean salinity).

³ The accurate data is available from <http://www.teos-10.org>.

192

193 By solving Equation 3, the free-falling droplet velocity variation from the release
194 in the static air is shown in Fig. 3 (the variation of v_a is discussed in section 4 in this
195 paper). Larger droplets tend to have a higher terminal velocity. The small differences
196 in droplet velocity between the present model and the model of Dehghani-Sanij et al.
197 [30] are due to the different C_d estimation. The velocity variations are in good
198 agreement with the experimental results conducted by Chowdhury, et al.[31]. The
199 experiment demonstrated that velocity of water drops grew very rapidly at the
200 beginning and reached to the peak (terminal) velocity after a very short time period and
201 distance. When the droplets reaching the peak (terminal) velocity, they no longer
202 accelerate and keep at this velocity constantly. The terminal velocities of falling water
203 droplets in the air are also demonstrated by many researchers in their experiments [32-
204 34].



205

206 Fig. 3. The freely-falling droplet velocity variation after the release in the static air.

207 3.2 A single water droplet freezing process

208 During the freezing process, the temperature inside of a droplet, in general, varies
209 with time and the position. To simplify and solve the transient heat transfer
210 phenomenon of water droplet, the Biot number, which is the ratio of heat convection at
211 the surface to the internal heat conduction of a body, is first evaluated.

$$212 \quad Bi = \frac{h_{conv} d}{k_d} \quad (5)$$

213 Where the h_{conv} is the convection heat transfer coefficient and the k_d is the
214 droplet (water or ice) thermal conductivity. A small Bi represents lower resistance to
215 conduction within a body. For $Bi < 0.1$, the temperature gradient within the droplet can
216 be neglected and uniform temperature within the body is regarded for the droplet.

217 One may notice that the Bi number would be slightly larger than 0.1 before the
218 phase change stage when the water droplet diameter is larger than 2.5mm. However, in
219 the calculation of Bi number, the circulation and mixing inside a freely falling water
220 droplet, which could enhance internal heat transfer within a body, is not considered yet.
221 The Reynolds number of the internal motion within a droplet is defined as [17, 35]:

$$222 \quad Re_{int} = \frac{v_a d}{2 \left(1 + \frac{\mu_w}{\mu_a}\right) \frac{\mu_w}{\rho_w}} \quad (6)$$

223 Where μ_w and μ_a is the dynamic viscosity of droplet and air, respectively.

224 Considering the internal motion, the effective thermal diffusivity is expressed as
225 [17, 35]:

$$226 \quad \alpha_{w,eff} = \frac{k_w}{\rho_w C_{p,w}^L} = \alpha_w (1 + 0.01 Re_{int}) \quad (7)$$

227 The $\alpha_{w,eff}$ is more than 10 times larger than the α_w of non-internal-motion
228 seawater, which means that the effective thermal conductivity k_w is much larger. Thus,
229 even if the water droplet is bigger than 2.5mm, the Bi number is still smaller than 0.1
230 if the internal motion within the droplet is considered. Furthermore, the thermal
231 conductivity of ice is about four times larger than that of seawater α_w , the Bi number
232 is still smaller than 0.1 when the ice is formed. Hindmarsh, et al. [36] also demonstrated
233 that a simple heat balance model is sufficient for the purpose of solving the internal
234 energy balance of the droplet, giving accurate results. Therefore, the temperature
235 gradient within the droplet is neglected in the whole freezing process of a droplet in
236 this paper and a simple heat balance model was used.

237 The freezing process of a droplet can be divided into four stages: initial (liquid)
238 supercooling, recalescence, solidification (phase change), and post-solidification (solid)
239 stage [36, 37]. The theory was based on that the liquid droplet will not crystallize until
240 it is supercooled and reaches the nucleation temperature T_n which is much lower than
241 the freezing temperature T_f . Once the first crystal nuclei are formed, a rapid

242 crystallization happens, resulting in a sudden temperature rise from T_n to T_f , which
 243 is called the recalescence stage.

244 The droplet continuously releases heat during its freezing process, the total energy
 245 released includes the convective heat loss, radiative heat loss, and evaporative heat loss:

$$246 \quad q_{total} = q_{conv} + q_{rad} + q_{evap} \quad (8)$$

$$247 \quad q_{conv} = h_{conv}(T_d - T_a) \quad (9)$$

$$248 \quad q_{rad} = \varepsilon\sigma(T_d^4 - T_a^4) \quad (10)$$

$$249 \quad q_{evap} = h_{mass}(Y_{w,i} - Y_w)\Delta H_v \quad (11)$$

$$250 \quad Y_{w,i} = 0.622 \frac{P_{w,sat}}{P - P_{w,sat}} \quad (12)$$

251 Where the T_d is droplet (water or ice) temperature, T_a is the atmosphere temperature,
 252 σ is the Stefan-Boltzmann constant, ε is the droplet emissivity. $Y_{w,i}$ is the humidity
 253 mass ratio of saturated moist air at the water-air interface, which depends on the droplet
 254 temperature T_d . Y_w is the humidity mass ratio of moist atmospheric air.

255 The convective heat and mass transfer coefficient h_{conv} and k_{mass} were
 256 obtained from experimental data by Ranz and Marshall [38]:

$$257 \quad N_u = \frac{h_{conv}d}{k_a} = 2 + 0.6P_r^{1/3}R_e^{1/2} \quad (13)$$

$$258 \quad S_h = \frac{h_{mass}d}{D_{w,a}} = 2 + 0.6S_c^{1/3}R_e^{1/2} \quad (14)$$

259 where N_u is Nusselt number, P_r is Prandtl number $P_r = \mu_a/\rho_a\alpha_a$, S_h is Sherwood
 260 number, S_c is Schmidt number $S_c = \mu_a/\rho_aD_{w,a}$, R_e is the Reynolds number.

261 Due to the mass transfer, the droplet mass decreases continuously until the
 262 evaporation ends. The mass change of a droplet can be calculated by:

$$263 \quad (m_d)_t = h_{mass}(Y_{w,i} - Y_w)A_d\Delta t + (m_d)_{t+\Delta t} \quad (15)$$

$$264 \quad \frac{dm_d}{dt} = -h_{mass}(Y_{w,i} - Y_w)A_d \quad (16)$$

265 where m_d is the mass of a water droplet and the A_d is the surface area of a water
 266 droplet.

267 According to [16], when a droplet surface temperature reaches the freezing point,
 268 ice nucleation begins at the surface, a solid shell grows rapidly around the surface
 269 (about 2/30-3/30 s) and then solidifies inwards. The evaporative mass transfer from the
 270 water to the ambient air can be neglected during the ice formation process around the
 271 droplet surface.

272 Before the solidification (phase change) stage, the energy balance for the droplet
 273 is:

$$274 \quad (m_dH_d)_t = (m_dH_d)_{t+\Delta t} + A_dq_{conv}\Delta t + A_dq_{rad}\Delta t + A_dq_{evap}\Delta t \quad (17)$$

275 and the final expression for the water temperature T_d is

$$276 \quad \frac{dT_d}{dt} = - \frac{h_{conv}A_d(T_d - T_a) + \varepsilon\sigma(T_d^4 - T_a^4)A_d + h_{mass}(Y_{w,i} - Y_w)A_d\Delta H_v}{m_d C_{p,w}^L} \quad (18)$$

277 During the solidification (phase change) stage, the ice is formed from the outside
 278 and it pushes the impurities to the center of the drop, resulting in a higher concentrated
 279 liquid and nearly pure ice. This concentrated solution would decrease the freezing
 280 temperature until the new equilibrium is reached. Thus, the heat released by the droplet
 281 will not only facilitate the phase change but also reduce the droplet (both the outside
 282 ice and the inside concentrated solution) temperature. Since the diffusion of impurities
 283 in the ice can be negligible [37, 39], the droplet temperature will follow the freezing
 284 point depression line (see Fig. 2). Based on this theory, the energy balance for the
 285 droplet is:

$$286 \quad (m_d H_d)_t = (m_d H_d)_{t+\Delta t} + A_d q_{conv} \Delta t + A_d q_{rad} \Delta t - \Delta H_s m_d f r_{ice} \quad (19)$$

287 and the final expression is:

$$288 \quad \Delta H_s m_d \frac{d f r_{ice}}{dt} - \left(C_{p,ice} m_d f r_{ice} + C_{p,w}^L m_d (1 - f r_{ice}) \right) \frac{dT_d}{dt} = A_d q_{conv} + A_d q_{rad} \quad (20)$$

289 where $f r_{ice}$ is the ice mass fraction in the droplet, ΔH_s is the specific latent heat of
 290 fusion.

291 Equation 19 could be solved with the freezing point depression equation (Equation
 292 1 for seawater) with a forward difference time step method [37] or a chain rule method
 293 [39]:

$$294 \quad \frac{dT_d}{dt} = \frac{dT_d}{d f r_{ice}} \frac{d f r_{ice}}{dt} = \frac{dT_f}{d f r_{ice}} \frac{d f r_{ice}}{dt} \quad (21)$$

295 For seawater, when the ice appears, the freezing point could be expressed as:

$$296 \quad T_f = -54.1126 \left(\frac{S_w / (1 - f r_{ice})}{1 - S_w / (1 - f r_{ice})} \right) \quad (22)$$

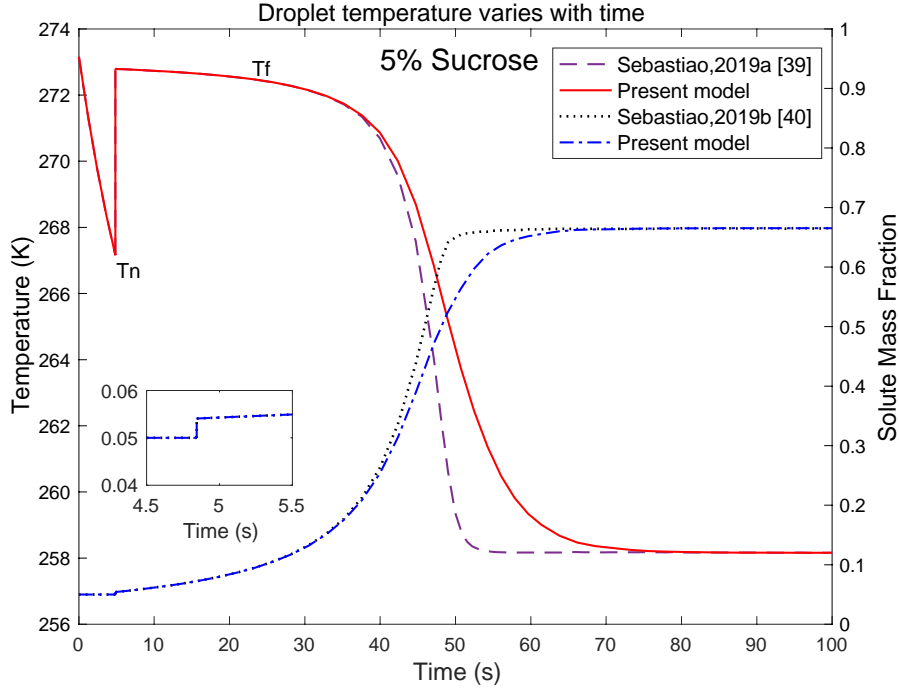
297 where S_w is the initial salinity of the seawater before crystallization.

298 The phase change stage ends when the temperature of the droplet or the
 299 concentration of the inside solute reaches the eutectic point (23.3% for seawater). After
 300 that the post- solidification stage starts. The droplet temperature can be expressed as:

$$301 \quad \frac{dT_d}{dt} = - \frac{h_{conv}A_d(T_d - T_a) + \varepsilon\sigma(T_d^4 - T_a^4)A_d}{C_{p,ice} m_d f r_{ice} + C_{p,w}^L m_d (1 - f r_{ice})} \quad (23)$$

302 To validate this numerical model, the freezing process of a sucrose droplet was
 303 simulated. The comparison with the reference [39] and [40] was made in Figure 4. In
 304 [39], the temperature variation of a solution droplet during the freezing process was
 305 discussed. The solute mass fraction was analyzed in the following paper [40]. The
 306 boundary conditions were: $T_a = -15^\circ\text{C}$, $d = 1.56\text{mm}$, $v_a = 0.42\text{m/s}$, $v_w = 0\text{m/s}$. A
 307 slight difference between the model in the reference [39] and [40] with the present
 308 model was observed in this figure. In [39, 40] the temperature gradient of the surface
 309 ice was considered and the inside concentrated solution was treated as a lumped matter.

310 Thus, $C_{p,ice}m_d r_{ice}$ in Equation 20 was not calculated in those papers (see Equation
 311 20 in [39]). While, in this paper, as discussed before, the temperature gradient of the
 312 droplet (ice/water) was neglected, since the thermal conductivity of ice is about four
 313 times larger than the seawater. The protuberance of the solute mass fraction at the
 314 beginning of the freezing process (between 4.5-5s) was caused by the ice formed in the
 315 recalescence stage.



316
 317 Fig. 4. The freezing process of a 5% sucrose droplet

318 4. A system of droplets freeze in the tower

319 4.1 Collision and coalescence of water droplets

320 As discussed in the previous section, since the large droplets will reach a higher
 321 terminal velocity than that of the smaller droplets. When different diameters of water
 322 droplets are emitted by a spray nozzle, the larger droplets will collide with the smaller
 323 ones during the falling process in the tower. Some of the smaller droplets will be
 324 collected by the larger ones after the collision and resulting in coalescence. Those
 325 droplets collided without a coalescence will bounce away from each other. The
 326 probability of coalescence depends on the collision angle of two droplets [41].

327 The concept of Energy Tower that cools the hot desert air by spraying seawater
 328 on the top of the tower and thus generates a downdraft to produce power was proposed
 329 by [41]. In this paper, the collision frequency between two droplets with different
 330 velocity was expressed as:

$$331 \theta = N_1 N_2 \pi (d_1/2 + d_2/2)^2 |v_{w,1} - v_{w,2}| \quad (24)$$

332 where N is the number of droplets per unit volume, d is the droplet diameter, and the
 333 subscript 1 and 2 indicate different diameters of the droplets. The probability of
 334 coalescence is set to be 1/2. In this energy tower, the calculation indicates that the model

335 with collision consideration produced only 6% lesser energy (or the velocity of the
336 downdraft) in this 1000m-high tower compared with no collision consideration.

337 To simplify the mathematical process, the so-defined Sauter diameter was
338 proposed by Makkinejad [42] to replace all the droplets with different sizes by a
339 population of spherical uniform-size droplets in the tower (thus no collision would
340 happen). The equalized spherical droplet diameter is $d_s = \sum_i d_i^3 / \sum_i d_i^2$. It was found
341 that this model produces small deviations (<2.1%) in an industrial counter cooling
342 tower. Therefore, a population of spherical uniform-size drops was assumed in the
343 following section.

344

345 4.2 Heat and mass transfer between water droplets and air

346 Assumptions listed below are also suggested in this article:

347 1). The process is under the steady-state, which means the variables of the process
348 are unchanging in time under a given condition. The initial situation (a transient state
349 or a start-up period) is not considered;

350 2). One-dimensional compressible flow in the tower without crosswind;

351 3). The distribution of water and air mass flow is uniform inside the tower;

352 Since the freezing process of seawater can be divided into four stages, the tower
353 will also be separated into sections to calculate the parameters of the air. But it should
354 be noticed that the recalescence stage will not happen in the freely falling seawater
355 droplets because the nucleation temperature is slightly higher (0.3% ~ 0.4%) than the
356 freezing temperature [17]. Then the tower is divided into two parts: i) in the upper part,
357 the water droplets still stay above the freezing point. Heat and mass transfer happen
358 simultaneously in this part; ii) in the lower part, because of the solid shell, the mass
359 transfer from the water to the ambient air can be neglected when the ice is formed
360 quickly around the surface.

361 Llano-Restrepo [28] proposed a set of equations to numerically calculate the heat
362 and mass transfer between water and air in a spray cooling tower neglecting the
363 radiative heat transfer. Those equations transform the temperature gradient against the
364 time (s) to against z (m) by introducing L and A to substitute the m_d and A_d ,
365 respectively. In the following equations, z is the vertical distance from the bottom of
366 a cooling tower upward, G_B is the mass flow rate of dry air per unit cross-section area
367 of the cooling tower ($kg/m^2 \cdot s$), L is the water mass flow rate per unit cross-section
368 area of the cooling tower $kg/m^2 \cdot s$, A is the interfacial area per tower unit
369 volume (m^2/m^3), $A = N \cdot \pi d^2$, and N is the number of water drops falling through a
370 unit volume per second, $N = 6L/\rho_w \pi v_w d^3$. With the addition of the radiative heat
371 transfer, those equations were given below, a more comprehensive analysis can be
372 found in [28]:

373 for the humidity mass ratio, Y_w is:

374
$$\frac{dY_w}{dz} = h_{mass}(Y_{w,i} - Y_w)A/G_B \quad (25)$$

375 for the water mass flow rate, L is

376
$$\frac{dL}{dz} = h_{mass}(Y_{w,i} - Y_w)A \quad (26)$$

377 for the air temperature, T_a is

378
$$\frac{dT_a}{dz} = \frac{h_{conv}A(T_w - T_a) + \varepsilon\sigma(T_w^4 - T_a^4)A + h_{mass}(Y_{w,i} - Y_w)A \int_{T_a}^{T_w} C_{p,w}^g dT}{G_B(C_{p,B} + Y_w C_{p,w}^g)} \quad (27)$$

379 for the water temperature, T_L is

380
$$\frac{dT_w}{dz} = \frac{h_{conv}A(T_w - T_a) + \varepsilon\sigma(T_w^4 - T_a^4)A + h_{mass}(Y_{w,i} - Y_w)A\Delta H_v}{LC_{p,w}^L} \quad (28)$$

381 Equations 25, 26 and 28 can be used for water droplets before the phase change
 382 stage in the tower (it should be noticed that the minus sign was not shown in Equations
 383 26 and 28 because of the differential direction). During the phase change stage, one can
 384 easily transform Equations 19-21 from $\frac{dT_w}{dt}$ to $\frac{dT_w}{dz}$. But the Equation 27 that treated
 385 the air as incompressible gas without considering the variations of air density and air
 386 pressure in the cooling tower is not suitable for the model in this paper, because the
 387 continuous density change of air in this model is the main reason for the formation of
 388 natural draught during the seawater droplets freezing. And the volume of airflow
 389 dominates the maximum quantity of seawater that can be frozen in the tower (see the
 390 discussion section).

391 To solve the one-dimensional compressible airflow in a high tower, a method for
 392 calculating this buoyant flow induced by the variation of air density was proposed in
 393 [43], validated by [44] and further developed by [45]. But the forces that coupling
 394 between discrete water droplets and continuous air were not considered in those models,
 395 which are not neglected in the model of this paper. The new method considering the
 396 forces from water droplets and the heat/mass transfer between water and air is
 397 expressed into two parts according to the freezing stage of the droplets:

398 1). During the phase change stage of the seawater droplets:

399 The state equation of air:

400
$$\frac{dP}{P} - \frac{d\rho_a}{\rho_a} - \frac{dT_a}{T_a} = 0 \quad (29)$$

401 The continuity equation of air after the water droplets fell below freezing
 402 temperature:

403
$$d(\rho_a v_a S) = 0 \Rightarrow \frac{d\rho_a}{\rho_a} + \frac{dv_a}{v_a} = 0 \quad (30)$$

404 The momentum equation of air:

405
$$dP + \rho_a v_a dv_a + \rho_a g dz + \frac{\lambda}{D} \cdot \frac{\rho_a v_a^2}{2} \cdot dz + F_w dz = 0 \quad (31)$$

406 where λ is the friction coefficient on the wall of the tower, $\lambda = 0.008428$ [43],

407 F_w is the source term of momentum due to the forces of water droplets.

408 The F_w was given in [46] as:

$$409 \quad F_w dz = \frac{dv_w}{dt} \frac{m_w dt}{dV} dz = \frac{dv_w}{dt} \frac{L \cdot S \cdot dt}{dV} dz = \frac{dv_w}{dt} \frac{L}{dz/dt} dz = \frac{dv_w}{dt} \frac{L}{v_w + v_a} dz \quad (32)$$

410 where m_w is the water mass flow rate kg/s , dV is the control volume, S is the
411 cross-section area of the tower m^2 .

412 To solve those equations, two more numbers were introduced:

413 Mach number is defined as the ratio of local velocity v and the speed of sound:

$$414 \quad M = \frac{v_a}{\sqrt{\gamma RT}} \quad (33)$$

415 where γ is the specific heat ratio of air, $\gamma = C_{p,a}/C_{v,a}$.

416 Froude number is defined as the ratio between inertial and gravity force:

$$417 \quad F_r = \frac{v_a}{\sqrt{gD}} \quad (34)$$

418 This momentum equation can be expressed finally as:

$$419 \quad \frac{dP}{P} + \gamma M^2 \frac{dv_a}{v_a} = -\gamma M^2 \cdot \frac{2}{\lambda F^2} \cdot \frac{\lambda}{2D} dz - \gamma M^2 \cdot \frac{\lambda}{2D} dz - \frac{F_w dz}{P} \quad (35)$$

420 To make the formulae read easily, a shorthand for the right-hand side of Equation
421 35 is introduced as MoX.

422 The energy equation of air per unit mass:

$$423 \quad dW - dQ + dH + v_a dv_a + gdz = 0 \quad (36)$$

424 where W is the work, Q is the heat transferred during the height of dz , H is the
425 enthalpy.

426 Since the work is zero, this equation can be rewritten as:

$$427 \quad C_p dT_a + v_a dv_a + gdz = dQ \quad (37)$$

428 With neglecting mass transfer:

$$429 \quad dQ = dQ_{ice} = \frac{[q_{conv} + q_{rad}]A - \pi D q_{wal}}{G_B} dz \quad (38)$$

430 where dQ_{ice} is heat transferred from water droplets during the phase change stage.

431 q_{wal} is the heat loss of the air through the tower wall and can be expressed as [47]:

$$432 \quad q_{wal} = h_{wal} (T_a - T_{z,\infty}) \quad (39)$$

$$433 \quad Nu_{wal} = \frac{h_{wal} D}{k_a} = 0.023 Pr^{0.3} Re^{0.8} \quad (40)$$

434 where h_{wal} is the heat transfer coefficient, and $T_{z,\infty}$ is the temperature of the
435 atmosphere at the height z .

436 This energy equation can be expressed finally as:

$$437 \quad \frac{\gamma}{\gamma - 1} \cdot \frac{dT_a}{T_a} - \frac{dP}{P} = \gamma M^2 \cdot \frac{\lambda}{2D} dz + \frac{F_w dz}{P} + \frac{\rho_a dQ_{ice}}{P} \quad (41)$$

438 To make the formulae read easily, a shorthand for the right-hand side of Equation
439 41 is introduced as EX.

440 After solving Equations 29, 30, 35, and 41 above, we get:

$$441 \quad \frac{dT_a}{T_a} = \frac{\gamma - 1}{\gamma(M^2 - 1)} \cdot [(\gamma M^2 - 1) \cdot EX - MoX] \quad (42)$$

$$442 \quad \frac{dv_a}{v_a} = \frac{1}{\gamma(M^2 - 1)} \cdot [MoX - (\gamma - 1) \cdot EX] = -\frac{d\rho_a}{\rho_a} \quad (43)$$

$$443 \quad \frac{dP}{P} = \frac{\gamma - 1}{M^2 - 1} \cdot [M^2 \cdot EX - MoX/(\gamma - 1)] \quad (44)$$

444 $\frac{dT_a}{dz}$, $\frac{dv_a}{dz}$, and $\frac{dP}{dz}$ can be calculated from Equations 42, 43 and 44.

445 2). When the water droplets are still above freezing temperature, the continuity
446 equation of air can be rewritten as:

$$447 \quad d(\rho_a v_a) = dL \Rightarrow \frac{d\rho_a}{\rho_a} + \frac{dv_a}{v_a} = \frac{dL}{\rho_a v_a} = \frac{h_{mass} A (Y_{w,i} - Y_w)}{\rho_a v_a} dz \quad (45)$$

448 The energy equation is:

$$449 \quad \frac{\gamma}{\gamma - 1} \cdot \frac{dT_a}{T_a} - \frac{dP}{P} = \gamma M^2 \cdot \frac{\lambda}{2D} dz + \frac{F_w dz}{P} + \frac{\rho_a dQ_w}{P} \quad (46)$$

$$450 \quad dQ_w = \frac{A[q_{conv} + q_{rad} + q_{evap}] - \pi D q_{wal}}{G_B} dz \quad (47)$$

451 where dQ_w is heat transferred from water when water stayed above freezing
452 temperature.

453 To make the formulae read easily, a shorthand for the right-hand side of Equation
454 46 is introduced as EXw.

455 After solving Equations 29, 35, 45 and 46 above, we get:

$$456 \quad \frac{dT_a}{T_a} = \frac{\gamma - 1}{\gamma(M^2 - 1)} \cdot \left[(\gamma M^2 - 1) \cdot \left(EXw + \frac{dL}{\rho_a v_a} \right) - \left(MoX - \frac{dL}{\rho_a v_a} \right) \right] \quad (48)$$

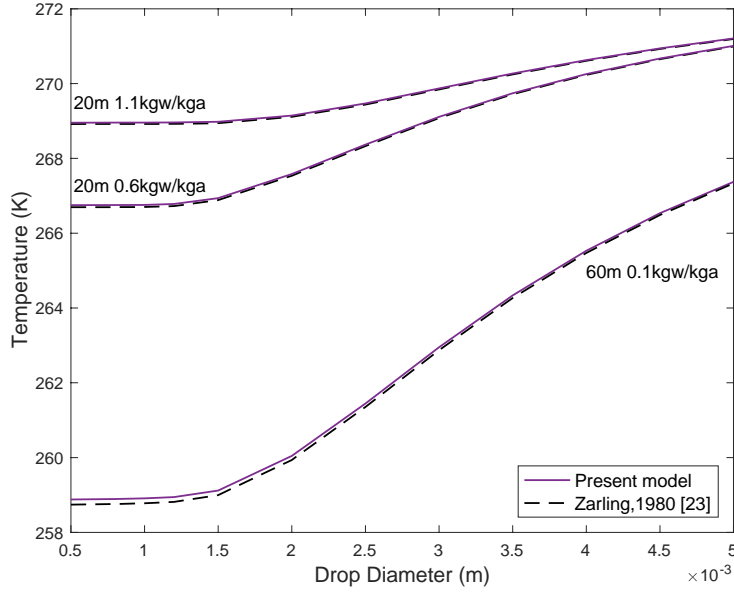
$$457 \quad \frac{dv_a}{v_a} = \frac{1}{\gamma(M^2 - 1)} \cdot \left[\left(MoX - \frac{dL}{\rho_a v_a} \right) - (\gamma - 1) \cdot \left(EXw + \frac{dL}{\rho_a v_a} \right) \right] \quad (49)$$

$$458 \quad \frac{dP}{P} = \frac{\gamma - 1}{M^2 - 1} \cdot \left[M^2 \cdot \left(EXw + \frac{dL}{\rho_a v_a} \right) - \left(MoX - \frac{dL}{\rho_a v_a} \right) / (\gamma - 1) \right] \quad (50)$$

459 $\frac{dT_a}{dz}$, $\frac{dv_a}{dz}$, and $\frac{dP}{dz}$ can be calculated from Equations 48, 49 and 50.

460 To validate this new method proposed in this paper, the temperatures calculated
461 by the present method are compared with those reported by Zarling [23] in Fig. 5. As
462 shown by Fig. 5, the variations of water temperature calculated by this new method are
463 in good agreement with the results reported in [25]. The slight difference may be caused
464 by different formulae used in two different methods (e.g. air/water viscosity, density
465 conductivity et al.). It should be noticed that the mass flow ratio of water (L) to air (G_B)
466 was set in that paper, but not by calculation. It can be seen that the temperature variation
467 of sprayed water is strongly affected by the flow ratio, which is also stated at the

468 beginning of this section.



469
470 Fig. 5. The final temperature of a system of water droplets freezing process

471 4.3 Energy generated by turbines

472 The pressure difference between the air inside the tower and the outside is the
473 integral of the product of the difference of the air densities by the gravity acceleration
474 with respect to height:

475
$$\Delta P_{pot} = g \int_0^h (\rho_{z,\infty} - \rho_z) dz = g \int_0^h \rho_{z,\infty} dz - g \sum_0^h \rho_z \Delta h \quad (51)$$

476 where h is the tower height, $\rho_{z,\infty}$ and ρ_z are ambient air density and internal airflow
477 density inside the tower at any height z, respectively. Although the air density in the
478 tower changes along with the tower height, this change can be neglected as long as the
479 Δh is small enough. In this paper, a proper value of 0.2m is selected for Δh .

480 According to the International Standard Atmosphere [48], environment air
481 temperature decreases with the altitude increasing. The temperature at altitude z meters
482 above sea level is approximated by the following formula (only valid no more than ~18
483 km above Earth's surface):

484
$$T_{z,\infty} = T_{0,\infty} - T_{la}z \quad (52)$$

485 The pressure at altitude z is given by:

486
$$P_{z,\infty} = P_{0,\infty} \left(1 - \frac{T_{la}z}{T_{0,\infty}} \right)^{g/RT_{la}} \quad (53)$$

487 The density of air can be calculated according to the ideal gas law:

488
$$\rho_{z,\infty} = \rho_{0,\infty} \left(1 - \frac{T_{la}z}{T_{0,\infty}} \right)^{(g/RT_{la}-1)} \quad (54)$$

489 where:

490 $P_{0,\infty}$ = sea-level standard atmospheric pressure, 101.325 kPa

491 $T_{0,\infty}$ = sea-level standard temperature, 288.15 K

492 T_{la} = temperature lapse rate, 0.0065 K/m

493 R = air specific constant, 287.05 J/(kg · K)

494 The specific potential energy due to heating is transformed to shaft power by
495 turbines, frictional losses in the tower, and lost to the environment. The total pressure
496 losses in the tower are the pressure potential minus ΔP_{turb} [49]:

$$497 \quad \Delta P_{loss} = \Delta P_{pot} - \Delta P_{tur} = \Delta P_{pot} - \zeta \Delta P_{pot} \quad (55)$$

$$498 \quad \Delta P_{loss} = \Delta P_{tur,in} + \Delta P_{br} + \Delta P_k \quad (56)$$

499 with

$$500 \quad \Delta P_{tur,in} = \varepsilon_{tur,in} \cdot \frac{1}{2} \rho_{a,in} v_{a,in}^2 \quad (57)$$

$$501 \quad \Delta P_{br} = \varepsilon_{br} \cdot \frac{1}{2} \rho_{a,in} v_{a,in}^2 \quad (58)$$

$$502 \quad \Delta P_t = \varepsilon_t \cdot \frac{1}{2} \rho_{a,out} v_{a,in}^2 \quad (59)$$

$$503 \quad \Delta P_k = \varepsilon_k \cdot \frac{1}{2} \rho_{a,out} v_{a,out}^2 \quad (60)$$

504 where ΔP_{turb} is the pressure drop at the turbine, ζ is the turbine pressure drop factor
505 which is defined as the ratio of the pressure drop at the turbine to the total pressure
506 potential. The ratio ζ is proposed to be 0.8 in [49], based on the previous work. In [49],
507 the pressure losses are suggested as: $\Delta P_{turb,in}$ is the turbine inlet pressure loss with
508 $\varepsilon_{turb,in} = 0.14$; ΔP_{br} is the pressure loss due to the internal bracing wheel (for
509 strengthening the tower) drag forces with $\varepsilon_{br} = 0.25$; ΔP_k is the pressure loss due to
510 exit kinetic energy loss with $\varepsilon_k = 1.26$. ΔP_t is the air collector-to-chimney (airflow
511 from horizontal to vertical) transition section pressure loss with $\varepsilon_t = 0.268$ [45].
512 $v_{a,in}$ and $v_{a,out}$ represent the velocity of air at the inlet and outlet of the tower
513 respectively.

514 According to [45], the airflow through the turbine can be treated as incompressible
515 air, which is accurate enough for a practical purpose. This indicates that the difference
516 in air density at the inlet and the outlet of the turbine can be neglected.

517 The power extracted from the turbine generators under a turbine load condition
518 can be expressed as:

$$519 \quad Pow_t = \eta \cdot \Delta P_{tur} \cdot S \cdot v_{a,in} \quad (61)$$

520 where η is the mechanical efficiency of the turbine generators, which is proposed to
521 be 77% in [49].

522

523 **5. Calculation procedure**

524 The whole calculation process is divided into three steps:

525 Step 1: A guessed value for seawater quantity that the desalination system could

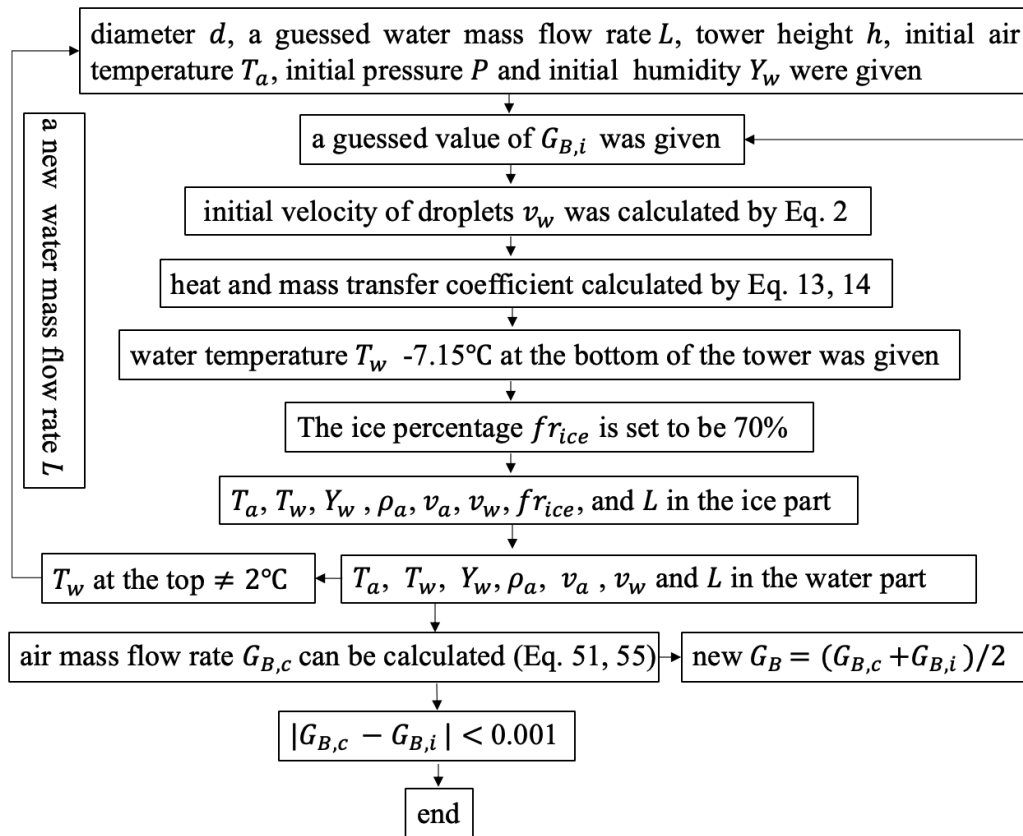
526 handle was given firstly, to calculate the corresponding flow of the cold air flowing into
 527 the tower. The differential equations were calculated from the bottom of the tower to
 528 the top of it.

529 Step 2: As the mass of the cold air induced into the tower by the pressure difference
 530 is not known, a guessed value for cold air mass flow rate was given for the iteration
 531 process. The Runge-Kutta fourth-order method [50] was applied to solve the Equations
 532 25, 26, 28, 48, 49 and 50 simultaneously for the upper part in the tower (before the
 533 phase change stage of the seawater). While for the lower (ice) part in the tower the
 534 Equations 26, 42, 43, 44 and the Equations 19-22 transformed from $\frac{dT_w}{dt}$ to $\frac{dT_w}{dz}$ need
 535 to be solved simultaneously. When these equations were solved, the temperature
 536 gradient against tower height was known. Then the mass of cold air can be calculated
 537 by Equations 51, 55 and 56. This value can be used as a reference value with the initial
 538 guessed value together to get a new G_B by Newton iteration method.

539 Step 3: This new G_B was used to recalculate the temperature variation of water
 540 droplets. If the water temperature on the top of the tower differed from the set
 541 temperature of 2°C, a new water mass flow rate would be suggested. This new water
 542 mass flow rate would be given to repeat step 1.

543 The final results would be obtained when the setting conditions were satisfied after
 544 steps 1 to 3. The whole calculation process is shown in the following figure.

545



546
 547

Fig. 6. The whole calculation process in this paper

548

549 **6. Results and discussion**

550 The experiments conducted by Gao [18, 51] showed that more than 60% of
551 impurity in the water was removed in the ice formed by the spray freezing. The ice was
552 about 70% of the total volume of feed water, while the rest was separated by gravity
553 and released as runoff. It was also demonstrated that a lower runoff fraction would
554 deteriorate the rate of impurity reduction because more brine pocket would be
555 entrapped in the ice powder. In another freeze desalination experiment [52], a mesh and
556 a filter cloth were used for gravity filtration of an ice slurry (a mixture of 1mm fine ice
557 grains and brine, ice fraction is more than 70%). Approximately 60% of the total feed
558 water was generated as the fresh water (at 0.5% NaCl concentration) after 50 min
559 filtration. Although the salinity of the generated water could be further lowered by
560 centrifugation, it is not discussed in this paper due to its energy consumption. From a
561 conservative point, the ice fraction after the spray freezing process was set to be 70%,
562 and 60% of the total feed water was assumed to be generated as fresh water. Thus, the
563 final temperature of water droplets is set to be -7.15°C based on Equation 21. The initial
564 seawater temperature was set to be 2°C , and the relative humidity of the atmosphere
565 was 80% [23].

566

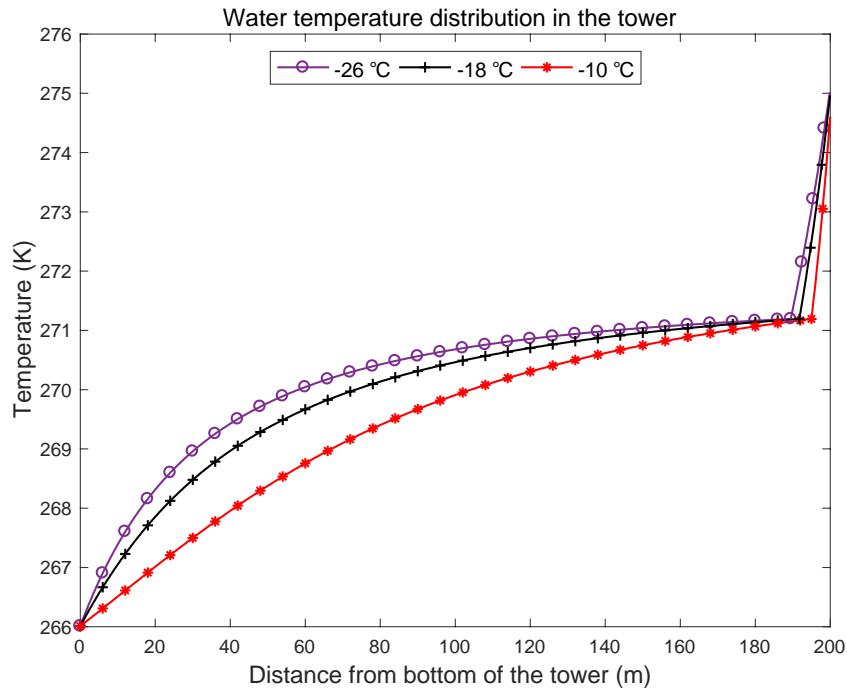
567 6.1 Impact of environmental temperature on system performance

568 The atmospheric air temperature variation can greatly influence system
569 performance. A spray freezing system with a 200m high tower under three different
570 surrounding environmental temperatures is analyzed first. The 2mm is chosen as the
571 Sauter diameter of the water droplets sprayed in the tower. It is reasonable because
572 more than 80% of the droplets had a diameter between 1mm to 2.8mm in the
573 experiments conducted by Gao [18, 51].

574 The variations of the water temperature are shown in Fig. 7. The typical
575 atmospheric temperature in the cold regions discussed in references is -26°C , -18°C , and
576 -10°C [17, 23, 30], those figures are also chosen in this paper. As stated above, the
577 water temperature at the top of the tower is set to be 2°C and it is set to be -7.15°C (70%
578 ice fraction) at the bottom. The longer distance of the water required to reach the
579 freezing point at -26°C is because of the larger mass flow ratio of feed water (L) to air
580 (G_B) in that condition. More water needs longer distances to freeze when the air mass
581 flow rate is smaller. The seawater requires a distance of 10.5m, 8.3m and 5.0m to reach
582 the freezing point at -26°C , -18°C , and -10°C , respectively and the corresponding mass
583 flow ratio of feed water to air is 0.089, 0.053, and 0.019, respectively (see Table 2).

584 Although a higher mass flow rate of the water releases more heat to the air, more water
 585 droplets also hamper the airflow in the tower due to the drag forces between the water
 586 droplet and the air. Thus, the mass flow rate of the induced air would not increase
 587 proportionally with the increase of the water quantity.

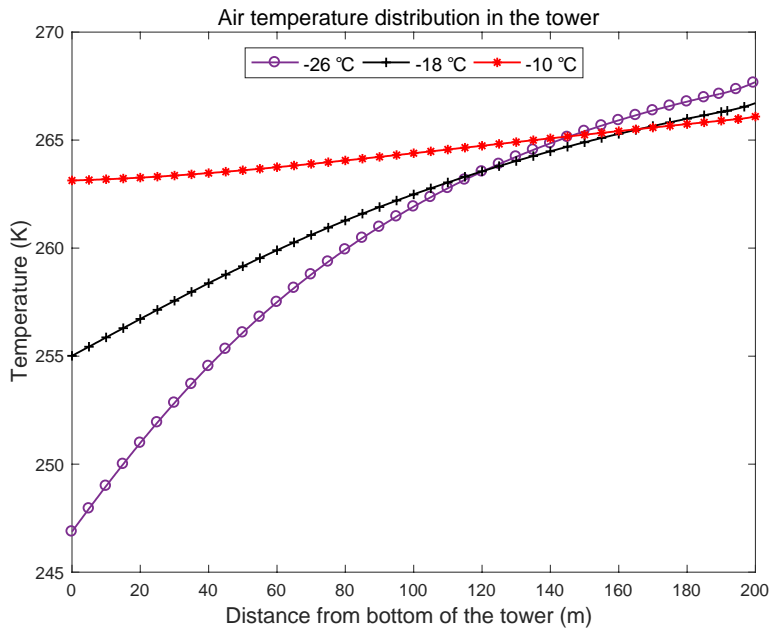
588 When the ice is developed on the surface of the droplet, higher concentrated water
 589 remains inside the droplet, leading to the reduction of its freezing point. Thus, the
 590 temperature of the droplets continuously decreases until it reaches 7.15 °C. The
 591 temperature decrease of water droplets is faster at -26°C at the lower half part of the
 592 tower (between the 0m to about 100m above the bottom) because of the large
 593 temperature difference between the cold air and water. At the height above 100m, the
 594 change of water temperature becomes smooth due to the small temperature difference
 595 between the cold air and water.



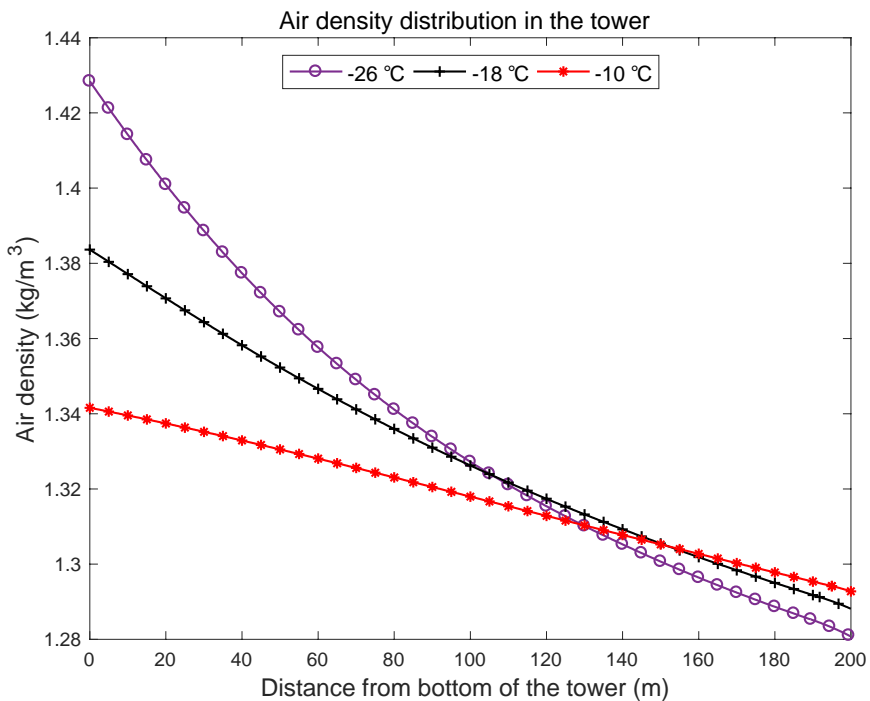
596
 597 Fig. 7. The temperature variations of water droplets during the freezing process in the system.
 598

599 The temperature and density variations of air in the tower are presented in Fig. 8
 600 and 9, respectively. Figs 8 and 9 show that a higher temperature difference between the
 601 air and water creates a higher heat transfer rate, a faster air temperature, and a higher
 602 rate of density change, especially during the lower half part of the tower. The final
 603 temperature of the air at the outlet of the tower is higher under the condition of the
 604 colder atmosphere, which is caused by a larger mass flow ratio of feed water (L) to air
 605 (G_B) in that condition. This feature is also reflected by the variations of density in Fig.
 606 9. The final density of the air is 1.281, 1.288, and 1.293 kg/m^3 at the atmospheric

607 temperature of $-26\text{ }^{\circ}\text{C}$, $-18\text{ }^{\circ}\text{C}$, and $-10\text{ }^{\circ}\text{C}$, respectively. The corresponding final
 608 temperature of the outlet air (200m above the bottom) is 267.7 K, 266.7 K, and 266.1K,
 609 respectively.



610
 611 Fig. 8. The temperature variations of the induced air in the tower at different atmospheric temperatures
 612



613
 614 Fig. 9. The density variations of the induced air in the tower at different atmospheric temperatures
 615

616 The main results of the freeze desalination system under different atmospheric
 617 temperatures are presented in Table 2. More air was induced into the tower to freeze

618 the sprayed water droplets in the colder atmosphere, which generated more fresh water.
 619 At the same time more power was generated by the turbine. The maximum of the
 620 generated fresh water flow rate was 27.7 kg/s at a temperature of -26°C . In this table,
 621 the fresh water generated was set to be 60% of the feed water and the mechanical
 622 efficiency of the pump for spray was set to be 0.85. The power consumption was
 623 calculated by $Pow_p = 0.85m_wgh$. The third column was the result from the second
 624 column multiplied with the cross-section area S and the fresh water generation rate
 625 60%.

Table 2

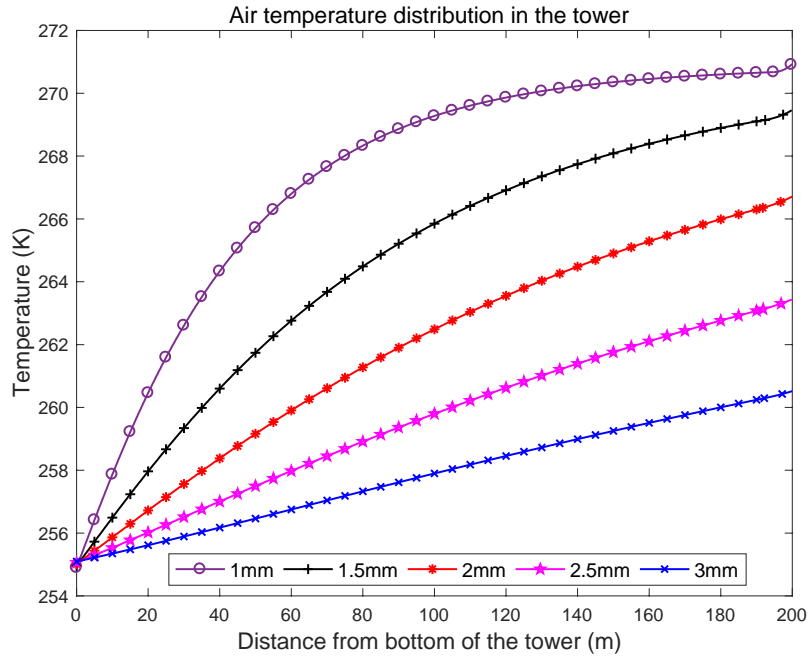
Results of the freeze desalination system under different atmospheric temperatures

Temperature	Feed water flow rate ($\text{kg/m}^2 \cdot \text{s}$)	Fresh water generated (kg/s)	Airflow rate ($\text{kg/m}^2 \cdot \text{s}$)	Power generation/ consumption
-26°C	0.587	27.70	6.62	30.35%
-18°C	0.243	11.45	4.58	25.96%
-10°C	0.038	1.80	2.00	14.66%

626

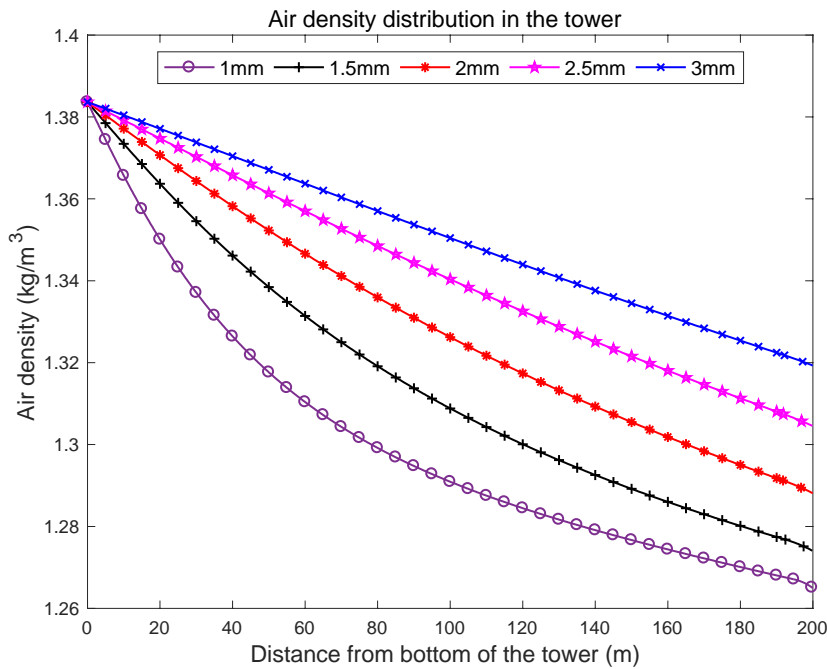
627 6.2 Impact of droplets' diameter on system performance

628 The variations of droplets' diameters can also greatly influence system
 629 performance. In the following discussion, the temperature of the surrounding
 630 atmosphere is set to be -18°C . The impact of droplets' diameters on air temperature and
 631 density is delineated in Fig. 10 and Fig. 11. As shown in Fig. 10, the air flows upwards
 632 from the bottom of the tower with a temperature rising. Compared to larger droplets,
 633 the temperature of air contacted with smaller droplets rises sharper at the beginning
 634 due to the larger area of heat transfer per unit mass. With the temperature difference
 635 between water and air being narrowed down quickly, the change of air temperature
 636 becomes slow and reaches a relatively "stable" state. This feature is also reflected by
 637 the variation of density in Fig. 11. The final density of the air is 1.265, 1.274, 1.288,
 638 1.305 and 1.319 kg/m^3 with the diameter of 1, 1.5, 2, 2.5 and 3mm , respectively.
 639 The corresponding final temperature of the outlet air (200m above the bottom) is
 640 270.9K, 269.5K, 266.7K, 263.4K and 260.5K, respectively. As discussed above, the
 641 final temperature of the outlet air would be higher when the droplets with smaller
 642 diameter sprayed into the tower, which is caused by the larger mass flow ratio of water
 643 to air (see Table 3).



644
645

Fig. 10. The temperature variations of the induced air in the tower with different droplets' diameters



646

647

Fig. 11. The density variations of the induced air in the tower with different droplets' diameters

648

649

650

651

652

653

The mass flow rate of the feed water that can be frozen by this system with different diameters of water droplets is present in Table 3. As expected, the water mass flow rate frozen by the system would be larger when smaller droplets sprayed into the tower because the smaller droplets have larger heat and mass transfer area per unit mass. Smaller droplets would also induce more air into the tower and generate more power. Though smaller droplets led to greater output (fresh water and power generated)

654 compared to larger droplets, smaller droplets needed greater water pressure produced
 655 by the pump and were prone to jam in the sprinkler. Too small droplets may endure the
 656 risk of being blown out of the tower by the updraft air, which resulted in water loss.
 657 Those advantages and disadvantages of using smaller droplets should be traded off in
 658 a real project.

Table 3

Results of the freeze desalination system with different diameters of water droplets

Droplets diameter	Feed water flow rate ($kg/m^2 \cdot s$)	Fresh water generated (kg/s)	Airflow rate ($kg/m^2 \cdot s$)	Power generation/ consumption
1mm	0.436	20.54	6.14	34.85%
1.5mm	0.349	16.44	5.40	29.61%
2mm	0.243	11.45	4.58	25.96%
2.5mm	0.150	7.07	3.75	23.05%
3mm	0.084	3.96	2.96	20.23%

659

660 From Table 2 and Table 3, it can be observed that the ratio of water mass flow rate
 661 to air mass flow rate was adjusted with the variation of the outside parameters. It cannot
 662 be set in this natural airflow induced by the pressure difference. The airflow rate is one
 663 of the most important factors that affect the fresh water output. The power generated
 664 by the air from turbines can compensate as large as one-third of the pump energy
 665 consumption, which was not recognized in previous research.

666

667 6.3 Limitations

668 Although a new mathematical model has been developed for heat and mass
 669 transfer between compressible airflow and water droplets freezing in a tall tower, there
 670 were some limitations in this model which could be improved in further study. Firstly,
 671 the wind effects were not considered in this paper. Wind from the surrounding
 672 environment may significantly affect the performance. It may blow the hot air from the
 673 top of the tower down to the bottom. Secondly, in this study water droplets sprayed by
 674 nozzle were treated as a population of spherical uniform-size droplets. Actually, the
 675 droplets from the nozzle may not be in a uniform shape. The droplets collide and bounce
 676 with each other due to the different velocities. The turbulent flow of the air and the
 677 momentum transfer during the collision need to be analyzed further.

678

679 7. Economic analysis of this spray freeze desalination system

680 In this economic analysis, the case of water droplets with a diameter of 2 mm
 681 sprayed in the atmospheric temperature of $-26^{\circ}C$ was taken for comparison with other
 682 desalination methods in the following part.

683 Firstly, this new spray freeze desalination method needs lesser power consumption

684 than some traditional methods. The power consumption required to produce 1 m^3
685 fresh water in this system is approximately 1.07 kWh , in which pump consumption is
686 the major part of the operational energy cost. Considering the power generated by the
687 turbines, this cost could be even lower by one third. If the altitude of the brackish water
688 is above the height of the desalination system (e.g. the tailing water at a mine), a pipe
689 could be made to channel the water to the tower and then benefit the operational cost
690 of this freeze desalination system. In comparison, to produce 1 m^3 fresh water, a
691 typical multi-stage flash distillation method needs 3.5 kWh power [53], the reverse
692 osmosis method consumes 2-8 kWh power [7].

693 Secondly, this new spray freeze desalination method is more energy-efficient than
694 other freeze desalination methods because of the high rate of heat and mass transfer
695 between the water droplets and the air. A direct contact type seawater freeze
696 desalination method was developed in [54]. In this experiment, a flow of refrigerant
697 cooled by the cold energy from the regasification of LNG was injected into a seawater
698 tank to generate ice. A technical and economic evaluation of this system was made by
699 [55]. The optimum result of this system was that it generated 1.64 kg/s fresh water
700 by consuming 7.83 kg/s seawater while the cold energy was provided by 1 kg/s
701 LNG regasification (about 827 kJ/kg energy would be released by the LNG). Thus,
702 the cold energy needed in this system was 504.3 kJ per kilogram fresh water. But in
703 the new freezing system proposed in this paper, only 375.4 kJ cold energy (calculated
704 from the enthalpy change of the airflow) was needed for generating one kilogram of
705 fresh water. A freezing crystallizer proposed by Attia et al. [56] needs 420 kJ energy
706 and a disk column freezing crystallizer developed by Van der Ham et al. [15] needs
707 1037-1282 kJ energy to produce 1 kg fresh water. From this point, if there is free
708 cold energy, the cold air (from the atmosphere or produced during the regasification of
709 LNG) can be utilized in the desalination system proposed in this paper which is more
710 energy-efficient than previous desalination systems discussed above.

711 Finally, according to the statistics data in [55], the price is about 1.5 USD for 1
712 m^3 freshwater and the industrial electricity price is about 0.15 USD for 1 kWh power.
713 The total fresh water generated by this system is 873,547 m^3 per year under the
714 assumption of no interruption of the free cold energy supply. The profit calculated by
715 deduction between the fresh water income and the pump cost is about 1,179,288 USD
716 per year (1,218,598 USD per year with power generated by the turbine). While the
717 construction cost of a 200m tower is about 5-10 million USD [57] depended on the
718 location, labor force cost and the materials of the tower. Then the feedback period of
719 this desalination system is about 4-8 years.

720

721 **8. Conclusions**

722 This paper investigated the feasibility of using spray freezing mechanism in a cold

723 environment to desalinate seawater. Because of the low energy consumption, no need
724 for huge pressure or membrane replacement work, and ignorable corrosion issues,
725 freeze desalination is an attractive method to desalinate the seawater. While, the spray
726 freezing method in this paper is more energy-efficient than the block, layer or falling
727 film freeze processes because it has higher heat and mass transfer area per unit seawater
728 and lower heat resistance.

729 In this paper, the freezing character of a freely falling seawater droplet was
730 analyzed first. The freezing process of a droplet was divided by several stages, the heat
731 and mass transfer of the droplet in each stage was investigated. An improved
732 mathematical method was proposed to numerically simulate this freezing process. Then
733 the heat, momentum, and mass transfer between a system of water droplets sprayed in
734 the desalination system and the natural convective airflow induced by the hot water
735 were studied. An iterative process to solve the proposed differential equations was
736 introduced in this paper.

737 The results demonstrated the seawater desalination capacity was affected by the
738 surrounding atmospheric temperature and the diameter of the water droplets. Colder
739 atmospheric temperature and smaller droplets produce more fresh water. The 200m
740 high desalination system could generate 27.7 kg/s fresh water (at 0.5% NaCl
741 concentration) with the 2mm diameter of the sprayed water droplet in the atmospheric
742 temperature of -26°C . The induced natural convective airflow could generate one-third
743 of the energy consumption of the water pump in this system, while this free energy was
744 never respected in previous research.

745 This new spray freeze desalination method consumes lesser power. The power
746 consumption required to produce 1 m^3 fresh water in this system is about 1.07 kWh .
747 With consideration of the power generated by the wind turbines, this cost could be even
748 lower by one third. Compared with some traditional desalination methods, the newly
749 proposed spray freeze desalination method consumes less power while the same mass
750 flow rate of fresh water is generated. This new method is also energy efficient compared
751 to other freeze desalination approach because of the direct contact between the cold and
752 warm flow (low heat resistance) and the large area of heat and mass transfer per unit
753 mass of water. It needs only 375.4 kJ cold energy to produce one-kilogram fresh water.

754 The spray freeze desalination process can generate fresh water and produce green
755 power simultaneously. It deserves to be considered by the desalination industry due to
756 its high efficiency if free cold energy is available. The economic analysis of the system
757 in different countries needs further study based on the local water, labor, electricity and
758 land prices in the next step.

759

760 **Acknowledgements**

761 This study is financially supported by the National Natural Science Foundation of

762 China (Grant No. 51778511), the Hubei Provincial Natural Science Foundation of
763 China (Grant No. 2018CFA029), the Key Project of ESI Discipline Development of
764 Wuhan University of Technology (WUT Grant No. 2017001), the Fundamental
765 Research Funds for the Central Universities (WUT Grant No. 2019IVB082), and the
766 Scientific Research Foundation of Wuhan University of Technology (No. 40120237).

767

768 **References**

- 769 [1] M.o.W. Resources. Water Resources in China.
770 <http://www.mwr.gov.cn/english/mainsubjects/201604/P020160406508110938538.pdf>.
771 2019
- 772 [2] H.R. Peyton, P.R. Johnson, C.E. Behlke. Saline Conversion and Ice Structures from
773 Artificially Grown Sea Ice. University of Alaska, Arctic Environmental Engineering
774 Laboratory and University of Alaska, Institute of Water Resources 1967.
- 775 [3] J. Chang, J. Zuo, K.-J. Lu, T.-S. Chung. Freeze desalination of seawater using LNG
776 cold energy. *Water Research*. 102 (2016) 282-93.
- 777 [4] P.M. Williams, M. Ahmad, B.S. Connolly, D.L. Oatley-Radcliffe. Technology for
778 freeze concentration in the desalination industry. *Desalination*. 356 (2015) 314-27.
- 779 [5] K. El Kadi, I. Janajreh. Desalination by Freeze Crystallization: An Overview. *The*
780 *International Journal of Thermal & Environmental Engineering (IJTEE)*. 15 (2017)
781 103-10.
- 782 [6] G. Naidu, X. Zhong, S. Vigneswaran. Comparison of membrane distillation and
783 freeze crystallizer as alternatives for reverse osmosis concentrate treatment.
784 *Desalination*. 427 (2018) 10-8.
- 785 [7] P. Byrne, L. Fournaison, A. Delahaye, Y. Ait Oumeziane, L. Serres, P. Loulergue, et
786 al. A review on the coupling of cooling, desalination and solar photovoltaic systems.
787 *Renewable and Sustainable Energy Reviews*. 47 (2015) 703-17.
- 788 [8] H. Yang, M. Fu, Z. Zhan, R. Wang, Y. Jiang. Study on combined freezing-based
789 desalination processes with microwave treatment. *Desalination*. 475 (2020) 114201.
- 790 [9] H. Shin, B. Kalista, S. Jeong, A. Jang. Optimization of simplified freeze desalination
791 with surface scraped freeze crystallizer for producing irrigation water without seeding.
792 *Desalination*. 452 (2019) 68-74.
- 793 [10] W. Tang, J. Tao, J.-a. Wang, C. Liu, H. Zhang. Sea ice desalination under gravity
794 using microwave heating. *Desalination*. 430 (2018) 159-64.
- 795 [11] W. Cao, C. Beggs, I.M. Mujtaba. Theoretical approach of freeze seawater
796 desalination on flake ice maker utilizing LNG cold energy. *Desalination*. 355 (2015)
797 22-32.
- 798 [12] P. Wang, T.S. Chung. A conceptual demonstration of freeze desalination-
799 membrane distillation (FD-MD) hybrid desalination process utilizing liquefied natural
800 gas (LNG) cold energy. *Water Research*. 46 (2012) 4037-52.

- 801 [13] M. John, A. Häkkinen, M. Louhi-Kultanen. Purification efficiency of natural
802 freeze crystallization for urban wastewaters. *Cold Regions Science and Technology*.
803 170 (2020) 102953.
- 804 [14] F. van der Ham, G.J. Witkamp, J. de Graauw, G.M. van Rosmalen. Eutectic freeze
805 crystallization simultaneous formation and separation of two solid phases. *Journal of*
806 *Crystal Growth*. 198-199 (1999) 744-8.
- 807 [15] F. van der Ham, G.J. Witkamp, J. de Graauw, G.M. van Rosmalen. Eutectic freeze
808 crystallization: Application to process streams and waste water purification. *Chemical*
809 *Engineering and Processing: Process Intensification*. 37 (1998) 207-13.
- 810 [16] W. Gao, D.W. Smith, D.C. Segó. Freezing behavior of freely suspended industrial
811 wastewater droplets. *Cold Regions Science and Technology*. 31 (2000) 13-26.
- 812 [17] K.R. Sultana, K. Pope, L.S. Lam, Y.S. Muzychka. Phase change and droplet
813 dynamics for a free falling water droplet. *International Journal of Heat and Mass*
814 *Transfer*. 115 (2017) 461-70.
- 815 [18] W. Gao, D.W. Smith, D.C. Segó. Treatment of pulp mill and oil sands industrial
816 wastewaters by the partial spray freezing process. *Water Research*. 38 (2004) 579-84.
- 817 [19] K.W. Biggar, R. Donahue, D. Segó, M. Johnson, S. Birch. Spray freezing
818 decontamination of tailings water at the Colomac Mine. *Cold Regions Science and*
819 *Technology*. 42 (2005) 106-19.
- 820 [20] C. Tatarniuk, R. Donahue, D. Segó. Freeze separation of salt contaminated melt
821 water and sand wash water at snow storage and sand recycling facilities. *Cold Regions*
822 *Science and Technology*. 57 (2009) 61-6.
- 823 [21] J.r. Schlaich, R. Bergermann, W. Schiel, G. Weinrebe. Design of Commercial Solar
824 Updraft Tower Systems—Utilization of Solar Induced Convective Flows for Power
825 Generation. *Journal of Solar Energy Engineering*. 127 (2005) 117-24.
- 826 [22] M.M. Conde, M. Rovere, P. Gallo. Molecular dynamics simulations of freezing-
827 point depression of TIP4P/2005 water in solution with NaCl. *Journal of Molecular*
828 *Liquids*. 261 (2018) 513-9.
- 829 [23] A.R. Dehghani-Sanij, S. MacLachlan, G.F. Naterer, Y.S. Muzychka, R.D. Haynes,
830 V. Enjilela. Multistage cooling and freezing of a saline spherical water droplet.
831 *International Journal of Thermal Sciences*. 147 (2020) 106095.
- 832 [24] O.J. González Pedraza, J.J. Pacheco Ibarra, C. Rubio-Maya, S.R. Galván González,
833 J.A. Rangel Arista. Numerical study of the drift and evaporation of water droplets
834 cooled down by a forced stream of air. *Applied Thermal Engineering*. 142 (2018) 292-
835 302.
- 836 [25] J.P. Zarling. Heat and mass transfer from freely falling drops at low temperatures.
837 1980. p. 20.
- 838 [26] H. Cui, N. Li, J. Peng, J. Cheng, N. Zhang, Z. Wu. Modeling the particle
839 scavenging and thermal efficiencies of a heat absorbing scrubber. *Building and*
840 *Environment*. 111 (2017) 218-27.
- 841 [27] IOC, SCOR, IAPSO. The international thermodynamic equation of seawater –
842 2010: Calculation and use of thermodynamic properties. Intergovernmental

843 Oceanographic Commission 2010. p. 196.

844 [28] M. Llano-Restrepo, R. Monsalve-Reyes. Modeling and simulation of counterflow
845 wet-cooling towers and the accurate calculation and correlation of mass transfer
846 coefficients for thermal performance prediction. *International Journal of Refrigeration*.
847 74 (2017) 47-72.

848 [29] R.a.A.C.E. American Society of Heating, Inc. ASHRAE Handbook—
849 Fundamentals, N.E., Atlanta, 2013.

850 [30] A.R. Dehghani-Sanij, Y.S. Muzychka, G.F. Naterer. Droplet trajectory and thermal
851 analysis of impinging saline spray flow on marine platforms in cold seas and ocean
852 regions. *Ocean Engineering*. 148 (2018) 538-47.

853 [31] M.N. Chowdhury, F.Y. Testik, M.C. Hornack, A.A. Khan. Free fall of water drops
854 in laboratory rainfall simulations. *Atmospheric Research*. 168 (2016) 158-68.

855 [32] J.O. Laws. Measurements of the fall-velocity of water-drops and raindrops. *Eos*
856 *Transactions American Geophysical Union*. 22 (1941) 709–21.

857 [33] R. Gunn, G.D. Kinzer. The terminal velocity of fall for water droplets in stagnant
858 air. *Journal of Meteorology*. 6 (1949) 243-8.

859 [34] P.K. Wang, H.R. Pruppacher. Acceleration to Terminal Velocity of Cloud and
860 Raindrops. *Journal of Applied Meteorology*. 16 (1977) 275-80.

861 [35] S.-C. Yao, V.E. Schrock. Heat and Mass Transfer From Freely Falling Drops.
862 *Journal of Heat Transfer*. 98 (1976) 120-6.

863 [36] J.P. Hindmarsh, A.B. Russell, X.D. Chen. Experimental and numerical analysis of
864 the temperature transition of a suspended freezing water droplet. *International Journal*
865 *of Heat and Mass Transfer*. 46 (2003) 1199-213.

866 [37] J.P. Hindmarsh, A.B. Russell, X.D. Chen. Experimental and numerical analysis of
867 the temperature transition of a freezing food solution droplet. *Chemical Engineering*
868 *Science*. 59 (2004) 2503-15.

869 [38] W. E. Ranz, W.R. Jr. Marshall. Evaporation from drops—I-III 1952.

870 [39] I.B. Sebastião, B. Bhatnagar, S. Tchessalov, S. Ohtake, M. Plitzko, B. Luy, et al.
871 Bulk Dynamic Spray Freeze-Drying Part 1: Modeling of Droplet Cooling and Phase
872 Change. *Journal of Pharmaceutical Sciences*. 108 (2019) 2063-74.

873 [40] I.B. Sebastião, B. Bhatnagar, S. Tchessalov, S. Ohtake, M. Plitzko, B. Luy, et al.
874 Bulk Dynamic Spray Freeze-Drying Part 2: Model-Based Parametric Study for Spray-
875 Freezing Process Characterization. *Journal of Pharmaceutical Sciences*. 108 (2019)
876 2075-85.

877 [41] S. Hassid, I. Merksamer, R. Guetta. Energy Towers – The effect of droplet
878 coalescence on power and the environment. *Solar Energy*. 86 (2012) 1443-53.

879 [42] N. Makkinejad. Temperature profile in countercurrent/cocurrent spray towers. *Int*
880 *J Heat Mass Transfer*. 44 (2001) 14.

881 [43] T.W. von Backström, A.J. Gannon. Compressible Flow Through Solar Power Plant
882 Chimneys. *Journal of Solar Energy Engineering*. 122 (2000) 138.

883 [44] X. Zhou, J. Yang, B. Xiao, G. Hou, Y. Wu. Numerical Investigation of a
884 Compressible Flow Through a Solar Chimney. *Heat Transfer Engineering*. 30 (2009)

885 670-6.

886 [45] A.S. Ćoćić, V.D. Djordjević. One-dimensional analysis of compressible flow in
887 solar chimney power plants. *Solar Energy*. 135 (2016) 810-20.

888 [46] M. Lucas, P.J. Martínez, J. Ruiz, A.S. Kaiser, A. Viedma. On the influence of
889 psychrometric ambient conditions on cooling tower drift deposition. *International*
890 *Journal of Heat and Mass Transfer*. 53 (2010) 594-604.

891 [47] Y.A. Çengel, A.J. Ghajar. *Heat and Mass Transfer: Fundamentals & Applications*.
892 Fifth ed. McGraw-Hill 2015.

893 [48] Standard Atmosphere. International Organization for Standardization 1975.

894 [49] X. Zhou, Y. Xu, S. Yuan, R. Chen, B. Song. Pressure and power potential of sloped-
895 collector solar updraft tower power plant. *International Journal of Heat and Mass*
896 *Transfer*. 75 (2014) 450-61.

897 [50] S.C. Chapra. *Applied Numerical Methods with Matlab for Engineers*. Third
898 Edition ed. McGraw-Hill, New York, 2012.

899 [51] W. Gao, D.W. Smith, D.C. Segó. Spray freezing treatment of water from oil sands
900 tailing ponds. *Journal of Environmental Engineering and Science*. 2 (2003).

901 [52] D. Chen, C. Zhang, H. Rong, C. Wei, S. Gou. Experimental study on seawater
902 desalination through supercooled water dynamic ice making. *Desalination*. 476 (2020)
903 114233.

904 [53] Y. Zheng, K.B. Hatzell. Technoeconomic analysis of solar thermal desalination.
905 *Desalination*. 474 (2020) 114168.

906 [54] C. Xie, L. Zhang, Y. Liu, Q. Lv, G. Ruan, S.S. Hosseini. A direct contact type ice
907 generator for seawater freezing desalination using LNG cold energy. *Desalination*. 435
908 (2018) 293-300.

909 [55] C.-W. Ong, C.-L. Chen. Technical and economic evaluation of seawater freezing
910 desalination using liquefied natural gas. *Energy*. 181 (2019).

911 [56] A.A.A. Attia. New proposed system for freeze water desalination using auto
912 reversed R-22 vapor compression heat pump. *Desalination*. 254 (2010) 179-84.

913 [57] A. Ayoub, B. Gjorgiev, G. Sansavini. Cooling towers performance in a changing
914 climate: Techno-economic modeling and design optimization. *Energy*. 160 (2018)
915 1133-43.

916



Click here to access/download
RDM Data Profile XML
DataProfile_5115675.xml



Conflict of interests

The authors declare that they have no known competing financial interests or personal relationships that could have appeared to influence the work reported in this paper.

The authors declare the following financial interests/personal relationships which may be considered as potential competing interests:

Yang Liu^{1,2}, Tingzhen Ming^{1,3}, Yongjia Wu¹, Renaud de Richter⁴, Yueping Fang⁵, Nan Zhou³

1. School of Civil Engineering and Architecture, Wuhan University of Technology, Wuhan 430070, China.

2. Department of Mechatronic Engineering, Wuhan Business University, Wuhan, China.

3. China Energy Group, Environmental Energy Technologies Division, Lawrence Berkeley National Laboratory, 1 Cyclotron Road, Berkeley, CA 94720 USA.

4. Tour-Solaire.Fr, 8 Impasse des Papillons, F34090 Montpellier, France.

5. Centre for Research in the Built and Natural Environment, School of Energy, Construction and Environment, Coventry University, Priory Street, CV1 5FB Coventry, UK.

* Corresponding author signs on behalf of all authors.



Mar.27, 2020

Author contributions

Yang Liu: Data curation, Writing- Original draft preparation, Software.

Tingzhen Ming: Supervision, Conceptualization, Methodology.

Yongjia Wu: Validation, Investigation.

Renaud de Richter: Conceptualization, Writing- Reviewing.

Yueping Fang: Visualization, Writing- Reviewing and Editing.

Nan Zhou: Writing- Reviewing and Editing.